Available online at www.sciencedirect.com
ScienceDirect
Cement and Concrete Research 38 (2008) 159–174
Cement and Concrete Research

Engineering the bonding scheme in C–S–H: The iono-covalent framework

R.J.-M. Pellenq [a], N. Lequeux [b], H. van Damme [b,*]

[a] Centre de Recherche en Matière Condensée et Nanosciences, CNRS, Campus de Luminy, 13288 Marseille cedex 09, France
[b] Ecole Supérieure de Physique et de Chimie Industrielles, Physico-Chimie des Polymères et des Milieux Dispersés, UMR 7615 CNRS-ESPCI-UPMC, 10 rue Vauquelin, 75231 Paris cedex 05, France

Received 16 September 2007; accepted 18 September 2007

Abstract

On the basis of recent molecular simulation and experimental studies, we discuss two possible strategies for tuning the mechanical properties of cementitious materials by modifying the bonding scheme in the hydrates at molecular level. We focus the discussion on the calcium silicate hydrates (C–S–H). A first strategy would be based on the strengthening of the network of cohesion forces acting between the individual C–S–H lamellae or between their crystallites. Atomic scale simulations by *ab initio*, molecular dynamics and energy minimization techniques show that the iono-covalent forces between individual C–S–H layers or C–S–H layer stacks, separated by strongly localized calcium ions and water molecules, are orders of magnitude larger than the ionic correlation forces acting between C–S–H surfaces separated by nm- or multi-nm-thick layers of mobile water molecules and ions. The elastic properties derived from this iono-covalent bonding scheme are in good agreement with experimental values obtained by ultrasonic or statistical ("grid") nanoindentation techniques. The concept picture for C–S–H which follows is that of a crystalline semi-continuum, with dense domains ("crystallites" or "particles") iono-covalently bonded to each other, possibly entangled also, and embedded as long as the mesoscale porosity is water-saturated in a relatively weak attractive stress field due to fluctuating electrostatic forces. Depending on the size, the aspect ratio, and the turbostratic order of the crystallites, and also the composition of the interstitial solution, the relative importance of each contribution could be modified. This provides the basis for a better control of properties such as early age or long term strength development for instance. In this respect, the microstructure-properties relationships in clay minerals provide interesting leads, pointing to the importance of bonding continuity rather than bond strength.

A second strategy to tune the mechanical properties of cement systems, akin to a biomimetic approach, is to hybridize the hydrates by grafting organic moieties on the mineral lamellae. This can be achieved by controlled hydrolysis of organo-silane precursor mixtures or by performing the hydration of the anhydrous silicates in silanized polymer solutions. The outcome may be materials with improved fracture energy and larger strain at failure.

Keywords: Hydrates; CSH; Cohesion; Modulus; Molecular simulation

1. Introduction

The theme of the 12th International Congress on the Chemistry of Cement, held in Montréal in July 2007, was the search for a knowledge-based innovative approach in cement systems. Knowledge-based innovations can come from a variety of horizons, like a better understanding of the rheological behavior of complex granular mixtures, a better knowledge of small mineral particles thermodynamics, or a deeper understanding of the microstructure-durability relationships for instance. The present contribution is intended to provide food for thought on the possibility of tuning the mechanical performances of cement systems by engineering the bonding scheme in the hydrates, starting from atomic scale. In this approach, C–S–H is undoubtedly the main target since it is also the major source of cohesion in materials made from ordinary Portland cement.

A first possible strategy, which is expected to lead to a better control of stiffness and strength while maintaining an essentially brittle behaviour, could be the engineering of the forces and the spatial force distribution which are giving C–S–H its remarkable cohesion, in spite of its multiscale porous structure and in

* Corresponding author. Tel.: +33 1 40 79 44 19; fax: +33 1 40 79 46 86.
E-mail address: henri.vandamme@espci.fr (H. van Damme).

0008-8846/$ - see front matter © 2007 Elsevier Ltd. All rights reserved.
doi:10.1016/j.cemconres.2007.09.026

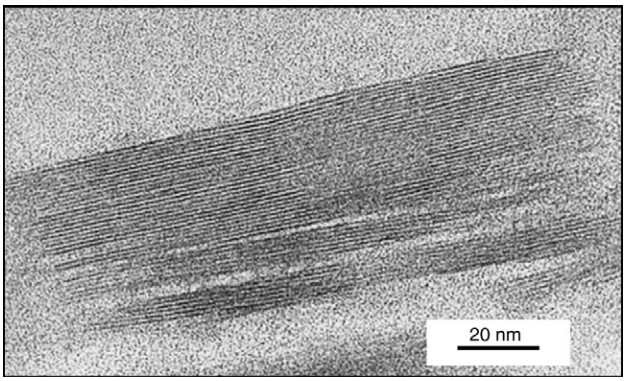

Fig. 1. TEM micrograph of C–S–H prepared by pouzzolanic reaction of calcium oxide with silicic acid at 60 °C for 100 days (Ca/Si = 0.9). Adapted from [3].

spite of the presence of water molecules between the individual nanoparticles. The prerequisite for this is a good knowledge of the nature of those forces and of the chemical parameters which are controlling them. Equally important is the understanding of the relationship between microstructure and the force (stress) network. In this respect, the microstructure-properties relationships in clay minerals provide interesting leads, pointing to the importance of bonding continuity rather than bond strength.

A second possible strategy, leading potentially to an increase of strength, toughness, and possibly to ductile behaviour, could be to hybridize the hydrates by introducing soft matter in the system. This strategy is extensively used by Nature whenever the fracture energy of an otherwise very brittle material, like calcite or aragonite for instance, has to be improved. Nacre is a well-known case which owes its toughness to the alternation of μm-thick hard and brittle aragonite crystals with nm-thick soft protein layers.

We are certainly not yet at the point where these strategies could be implemented in the real construction materials world, but the basis for it are being built. The point in the present paper is, first, to review our present knowledge of the cohesion forces in C–S–H, largely based on molecular simulation studies and, based on the conclusion that very short-range iono-covalent forces are essential, to think about possible ways to control the overall cohesion. Second, it will be shown that the use of sol–gel techniques and/or organo-mineral precursors opens a way towards the synthesis of truly hybrid hydrates.

2. Nano- and mesostructure of C–S–H

Our contribution to this issue is the companion paper of that of I.G. Richardson, in which the nanostructure of C–S–H is extensively discussed [1]. Therefore, we will not enter into a detailed review of the structural, spectroscopic or microscopic (mainly TEM) data which led to the current models for the atomic composition and structure of the individual lamellae. We will simply admit as established that the atomic structure of the smallest C–S–H unit is a layered crystal structure akin to that of the mineral tobermorite or to that of jennite, with a lamella thickness in the nm range [1,2]. This nm-thick lamellar structure is morphologically hardly recognizable in young hardened cement paste but it is evident from transmission electron microscopy (TEM) observations and X-ray diffraction patterns on pozzolanic C–S–H. Ordered stacks of up to several tens or even hundreds of nano-lamellae may be observed in some cases (Fig. 1).

Though less immediately obvious, the formation of ordered aggregates of C–S–H nano-lamellae may also be detected in hardened cement pastes or mortars or even concrete by high resolution TEM, especially in aged and/or well cured materials. Fig. 2, top, illustrates this for a heat-cured ultra-high performance matrix [4], but similar nanocrystalline regions may be detected in hardened OPC pastes (Fig. 2, bottom, and [5,6]).

The problem is to know how such locally anisotropic nanostructures assemble to form a basically isotropic material at larger length scales. C–S–H growth is not a simple process. Direct observation by AFM of C–S–H growth on alite, silica or calcite surfaces at the solid–solution interface reveals the initial formation of well individualized and more or less elongated 5 nm-thick disk-shaped particles with a long axis of the order of 60 nm [7,8]. Each particle is supposed to be an ordered stack of a few C–S–H lamellae, similar to those of the TEM micrograph of Fig. 1, but with a much less developed lateral extension. Interestingly, further hydration does not lead to growth of those particles but to their multiplication and to their aggregation,

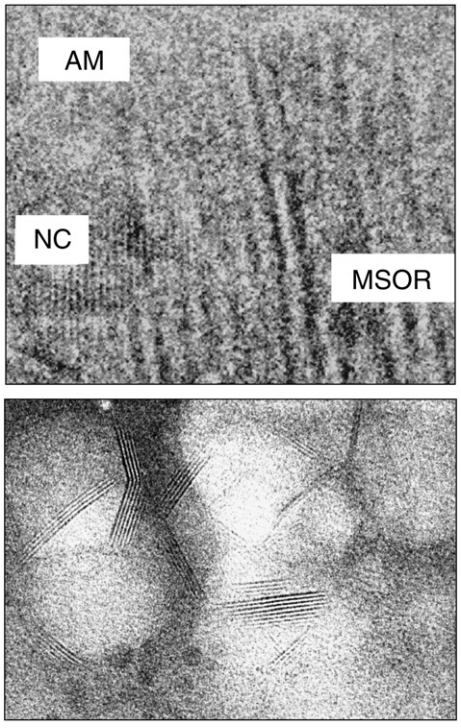

Fig. 2. Top: HRTEM micrograph of the C–S–H matrix in the paste of a ultra-high performance concrete cured at 90 °C for 24 hours. In addition to an amorphous matrix (AM), nanocrystalline regions (NC) are detected with periodicity between fringes in the nm domain, corresponding to stacks of C–S–H lamellae. Mesoscopically ordered regions (MSOR) with larger lattice parameters may also be detected (from [4]). Bottom: HRTEM micrograph of C–S–H in an OPC obtained with an environmental TEM instrument (Jeol 300 KeV) at 70% relative humidity (courtesy A. Baronnet, CRMCN, CNRS Marseille, France).

often along a preferred orientation. This leads to larger assemblies, with an incipient liquid crystalline organization. These assemblies may grow either laterally, parallel to the substrate surface, or axially, perpendicular to the surface. Lateral growth is always faster, but the ratio of axial over lateral growth depends on the lime concentration in the solution, large lime concentrations favouring the axial growth of high Ca/Si C–S–H [8,9]. The first layers of particles look remarkably well organized but, as the thickness of the layer increases, its roughness increases also and it tends to loose order. However, when aged in lime solutions, these disordered aggregated layers reorganize and yield almost atomically flat surfaces over areas of several μm^2 [10]. Such detailed and "live" observations can hardly be performed on dense cement or C_3S pastes. Nevertheless, by confining the paste close to a single crystal surface and removing the crystal after some time, hardened pastes with a flat surface could be obtained by Perez and Lesniewska [11]. In that case, AFM imaging reveals C–S–H particles very similar to those obtained upon hydrating single crystal surfaces with – remarkably – the same liquid crystalline ordering but, interestingly, with a smaller size (~40 nm instead of ~60 nm along the longest axis).

AFM is not the only imaging technique which shows the existence of small building blocks and orientational order. Bright field TEM of ultrathin (60 nm) sections of a resin-embedded hydrating C_3S paste shows compact aggregated nodules of approximately the same size as those observed by AFM [12]. Richardson [1,2,13,14] and Richardson and Groves [15–18], using direct bright field observation of samples on a grid, performed an extensive investigation of the morphology and structure of C–S–H in various hardened pastes including C_3S, C_2S, OPC, OPC-slag blends, KOH-activated or not, at room temperature or at 80 °C. A fine-textured and aggregated nodular structure could be observed in all materials, with typical nodule sizes ranging approximately from ~3 nm to ~10 nm. Most interesting is the difference between inner and outer products (Fig. 4) and, once more, the occurrence of a local orientational order typical of liquid crystalline behavior. The persistence length – that is, the distance over which a strand of nodules keeps the memory of its initial orientation – is much larger in the outer product. In aged or heat-cured samples, this leads to fibrils which can be several μm long and more than 100 nm wide. This corresponds to about a hundred stacked nano-lamellae. However, the (transverse) stacking order is far from perfect over such large distances.

What are the key microstructural features that should be retained from the previous brief review of C–S–H structure and morphology in order to build a realistic bonding scheme for a dense C–S–H hardened paste? Beyond the obvious multiscale nature of the problem, a general feature – so general that it is somewhat unexpected – is the ubiquitous presence of an orientational order. The ordered stacking of nano-lamellae along their c axis within the so-called particles, clearly visible in the special case of pozzolanic C–S–H (Fig. 1) and less clearly in dense pastes, is its first manifestation. More surprising is the alignment of the particles themselves in a nematic order (orientation order, no position order) when C–S–H is grown on or close to a single crystal surface (AFM images, Fig. 3), or in an edge-to-edge arrangement in dense pastes. The persistence length of these edge-to-edge alignments is particularly long in the outer product of aged materials, where it leads to long strands. The strands themselves organize more or less parallel to each other to form larger objects, the "fibrils" (or laths?), which can be seen in Fig. 4 (right). The alignment order of particles propagates over shorter distances (~100 nm) in the inner product. This can be interpreted in terms of shorter strand length or in terms of bending. Whatever the reason, it leads to a more homogeneous filling of space than what is achieved by the "fibrils" of outer product. An open question raised by these observations is the origin of the mesoscale order. It remains to be established whether it is due to chemical bonding or to pure excluded volume effects like in molecular or colloidal liquid crystals.

A bonding scheme taking into account the details of the complex structure just described – with organized objects at, at least, three different length scales – would be hardly tractable.

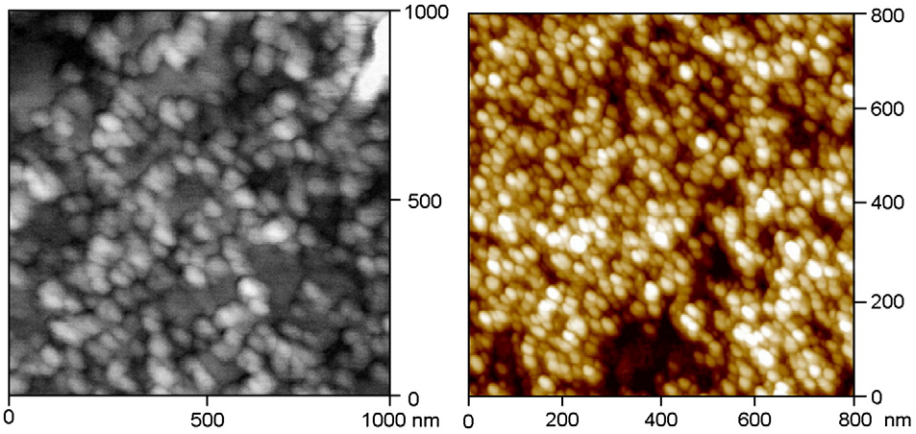

Fig. 3. AFM images of C–S–H nanoparticles grown on a flat (roughness smaller than 1 nm over 1 μm^2) silica slab at the silica–lime interface (left, from [8]), or on a cement paste in contact with a flat single crystal calcite surface (right, J.-P. Perez and E. Lesniewska, quoted in [11]). In the later case, the cement paste surface was imaged after removal of the calcite crystal. Note that the particles are smaller in the OPC paste than in the surface-grown C–S–H.

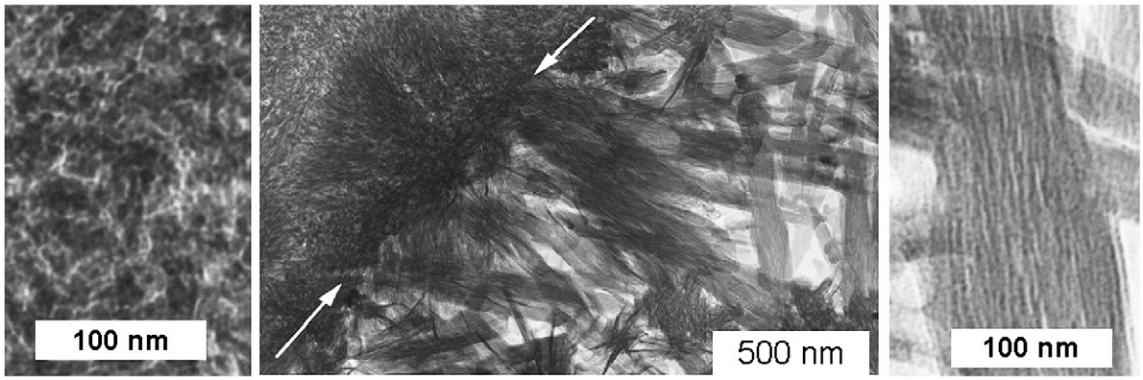

Fig. 4. Center: a TEM micrograph showing inner and outer products in a hardened C_3S paste prepared at w/c = 0.4 hydrated at 20 °C for 8 years. The white arrows indicate the inner-outer product boundary. Left and right: enlargements of inner (left) and outer (right) product regions, respectively (from [2], with permission). For more examples, the reader is referred to [1,2].

However, as far as "bond" nature or, in more general terms, attractive interactions are concerned, this complex structure may boil down to two or three types of model situations:

- A first model situation would be that of two parallel C–S–H lamellae separated by an interlamellar distance of the order of a few tenths of nm, i.e. of the same order as the interlayer distance in a tobermorite crystal with a 1.1 or 1.4 nm repeat distance for instance. This would happen within the "particles" detected by AFM and TEM where, presumably, a high lamellae stacking order exists, and also – most importantly – at the contact or, possibly, entanglement spots between those particles. The calcium ions in these very confined spaces, defined as "face-to-face" contacts, may be expected to be strongly interacting with the negative surface groups of the silica chains of the C–S–H lamellae and may be only partially hydrated. As a consequence, only atomistic approaches are able to model this type of situation properly.
- A second model situation is that of the more open domains (stacking defect regions) where pores of a few nm are separating the parallel or almost parallel C–S–H layers. A priori, a broad distribution of such distances is expected due to the packing disorder, but recent NMR data rather point to the existence of several narrow distributions [19]. The calcium ions in those more porous regions should be fully hydrated and highly mobile. As a consequence, less demanding molecular modelling methods can be applied, like those representing the pore water by a dielectric continuum for instance.
- A third model situation is that of the edge-to-edge contact between particles in the strands. Considering our poor knowledge of the edge chemistry of C–S–H lamellae, this is probably the most difficult situation to model.

More situations should be considered in order to build a complete picture of the bonding scheme in C–S–H, like edge-to-face for instance, or face-to-face in tilted orientation, but this is not a first priority considering the present state of our knowledge. We will restrict our approach to what seems to be the two main model configurations: face-to-face "contact" configurations on one hand, and face-to-face remote configurations on the other hand. A reasonable cartoon, from TEM micrographs, emphasizing continuity and entanglement, is shown in Fig. 5. The following sections are an analysis of the cohesion forces which may be acting in these two environments. As discussed elsewhere, van der Waals and capillary forces probably only contribute marginally to the cohesion of hardened cement [20]. We will therefore concentrate on the forces generated by the presence of charged surfaces and charged ions, starting from the mesoscale porous defect regions where a continuum approach is acceptable, and switching thereafter to the very confined sub-nano intra- and intercrystallites regions where a molecular description is compelling.

3. Cohesion at nano- and mesoscale

The electric double layer theory of Gouy and Chapman, based on the solution of the Poisson–Bolzmann equation, is almost a century old. This theory describes the formation of a diffuse electric double layer when a charged surface is in contact with an electrolyte solution. It permits also to calculate the interaction between two such surfaces facing each other. Combination of the GC or PB theory with van der Waals interactions led some sixty years ago to the so-called DLVO theory which is still the reference frame for many colloidal chemistry applications [21,22] and is extensively developed in textbooks [23,24]. The interaction between two identical particles, as predicted by the DLVO theory, is composed of two independent and additive parts: the double layer interaction, always repulsive, and the van der Waals interaction, always attractive.

It became increasingly clear in recent years that this was not correct and that a system composed of two charged particles with like charges may generate strongly attractive configurations due to correlations in the concentration fluctuations of counterions. This has been known for more than twenty years [25,26] and the suggestion that this may contribute to the cohesion of set cement has been made more than ten years ago [27]. The attraction appears when the electrostatic coupling in the electrolyte is sufficiently large. In aqueous media, this happens with divalent or multivalent ions at short separation, say in the nm range. With

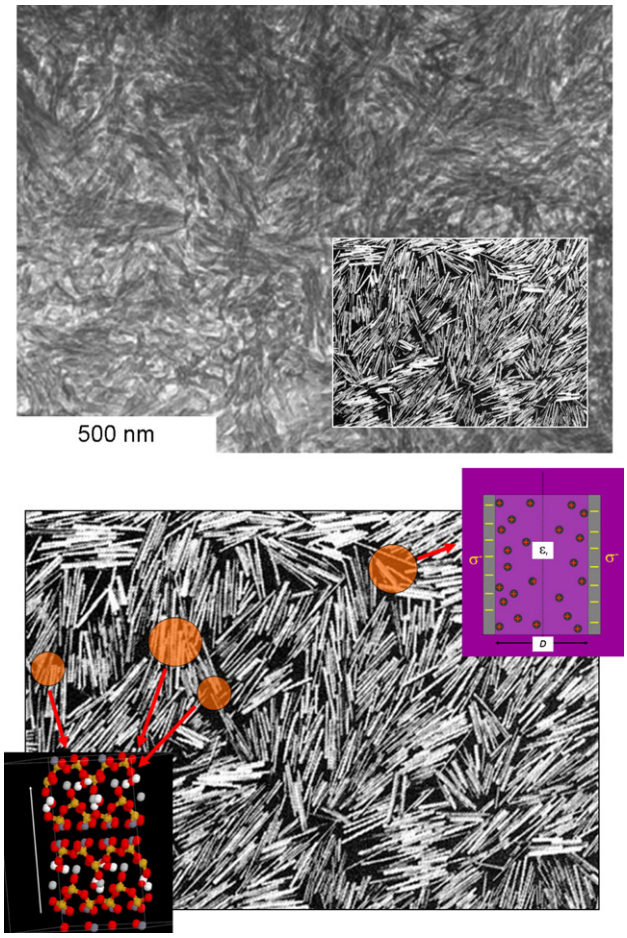

Fig. 5. Top: TEM micrograph of the inner product C–S–H in a hardened OPC paste prepared at w/c=0.4 and hydrated for 1 year at 20 °C (from [2], with permission). Inset: cartoon illustrating the type of imperfect liquid crystalline structure which could serve as model. Bottom: The same cartoon on which the two types of local situations to be modeled have been circled. On the left, three situations where C–S–H lamellae are in "contact", either within a stack (≅crystalline particle) or at contact spots between stacks, and where an atomistic description is compelling. On the right: a packing defect region where the distance between the lamellae forming the opposite pore surfaces is large enough to use a semi-continuum model.

monovalent ions, the double layer interaction is repulsive in most cases. The reason why the PB treatment and DLVO theory miss the possibility of attractive double layer interactions is the neglect of ionic concentration fluctuations. The PB equation is solved by assuming symmetry with respect to the mid-plane separating the two interacting objects. This is the so-called mean field approximation.

The first well documented example of attractive double layer interactions is the restricted swelling of Ca^{2+}-montmorillonite, compared to the Na^{+}-exchanged form. Montmorillonite belongs to the family of the so-called swelling or smectite clays [28,29]. The individual layers have a thickness similar to that of C–S–H layers, but their lateral extension is much larger, typically in the μm range (Fig. 6). The layers are negatively charged like in the case of C–S–H but the charge stems from ionic substitutions in the central octahedral backbone. Due to the screening of this deeply buried charge by the crystal lattice ions, the surface field

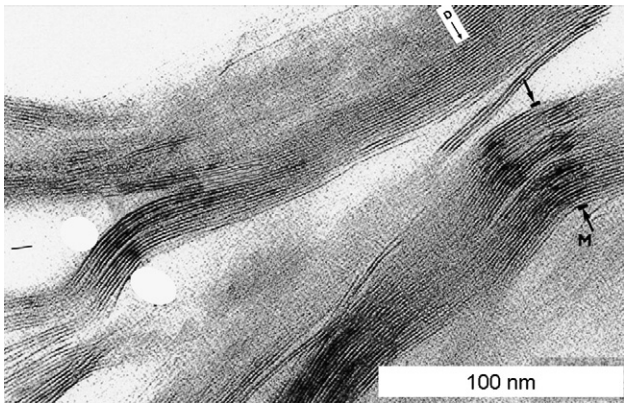

Fig. 6. TEM micrograph of a purified natural montmorillonite dispersed in water. The image was obtained on an ultrathin section, after solvent exchange and embedding in a resin. Note the much larger lateral extension of the lamellae as compared to C–S–H. Besides this, ordered stacks similar in thickness to those found in pouzzolanic C–S–H (Fig. 1) are observed. "D" indicates an edge dislocation (courtesy H. Gaboriau, C. Clinard, F. Bergaya and Ch.-H. Pons).

is expected to be much more diffuse than in C–S–H where the negative charge is stemming from the ionized silica tetrahedra at the lamellae surface.

As shown by Kjellander et al. [30,31], the restricted swelling of Ca^{2+}-montmorillonite is due to the so-called ionic correlation forces. In the Poisson–Boltzmann treatment of two identically charged surfaces with an intervening electrolyte solution, the two halves of the cell are symmetrical and both are neutral, so that no electric field is induced by one cell into the other. In a real system, the overwhelming majority of instantaneous ionic configurations do not achieve this ideal situation (Fig. 7). On the average, the electric field generated by one half of the lamellar system is still zero in the other half, but for every configuration there is a spatially varying field. The charges of

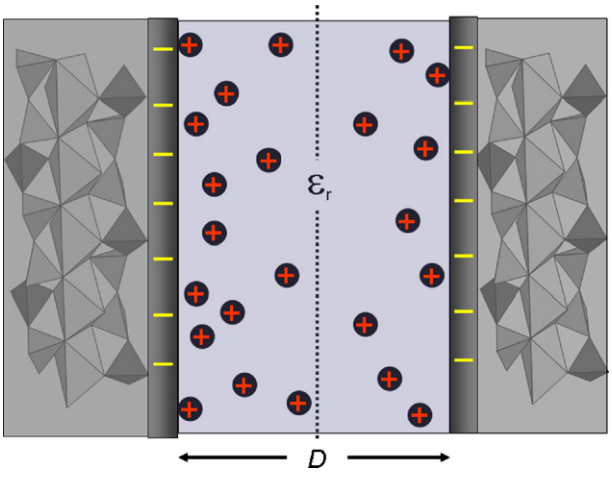

Fig. 7. Sketch of the model used to calculate double layer interactions by Monte Carlo simulation, using the so-called primitive model. The atomic structure of the C–S–H lamellae is ignored and replaced by uniformly charged walls separated by a dielectric continuum (water) in which hydrated ions are free to move. In the overwhelming majority of possible configurations, the distribution is neither symmetrical with respect to the mid-plane nor homogeneous along the vertical axis.

the second half respond to this instantaneous field by adopting configurations of lower energy, different from the mean field configuration. These correlated polarizations of the ionic clouds give rise to an ionic van der Waals type force, much in the same way as correlations between fluctuating electronic dipoles give rise to the London dispersion force.

Ionic correlation forces increase with the surface charge density and with the charge of the interlayer ions. Using Monte Carlo simulations in the NVT ensemble (constant temperature, volume, and number of ions in the interlayer space), Pellenq and co-workers [32–35] carried out a systematic study of correlation forces between charged planar surfaces in water in a broad range of charge densities, within the framework of the so-called primitive model (smooth flat surfaces separated by ions in a dielectric continuum). Charge densities going from less one charge per 2 nm^2 to one charge per 0.2 nm^2 were explored. The pressure was calculated for separation distances going from one to five hydrated ionic diameters. For the sake of comparison, both the case of Na^+ and Ca^{2+} counterions were studied. Neglecting van der Waals interactions, the z-component (z axis perpendicular to the surfaces) of the pressure can be written as the sum of three terms:

$$P_{\text{total}}(D) = P_{\text{elec}}(D) + P_{\text{contact}}(D) + P_{\text{ideal}}(D) \quad (1)$$

The first term is the force resulting from the sum of all the ion–ion, ion–lamella and lamella–lamella coulombic interactions through a plane at $z=0$ (mid-plane). Contrary to a widespread belief, this term is always attractive (negative), even in the mean field approximation. The Monte Carlo simulation, by exploring a large number of configurations, takes automatically into account the ionic correlations. The second, repulsive contact term is the hard core contact pressure, which is a consequence of using hydrated ions with a finite and realistic size, instead of point charges. It is proportional to the number of ions in contact (collisions) through the plane located at $z=0$ and takes automatically into account steric correlations. The third "ideal" term is nothing but the repulsive osmotic pressure, $\rho(0)$ kT, due to the kinetic contribution of the confined ions. It is obtained from the ionic density $\rho(0)$ in a volume of thickness δx around the mid-plane.

A first result is that the total ionic pressure is always repulsive with Na^+ counterions, even at the largest charge densities, showing that ionic correlations are negligible with small monovalent ions in water. The pressure values are also in good agreement, at moderate charge densities, with the mean field PB treatment. Second and more important, one or more attractive pressure wells were obtained with Ca^{2+} ions for all parameters sets investigated. For charge densities corresponding to montmorillonite (~ -0.7 e/nm^2), the pressure well is of the order of -1 MPa at a separation distance of 1.4 nm. But for a charge density corresponding to the theoretical charge of a C–S–H lamellae with all the OH groups of the silica chains ionized (at Ca/Si=1), that is ~ -3 e/nm^2, the depth of the well increases to -60 MPa at a separation of 0.7 nm, which is more than one order of magnitude larger than the van der Waals pressure at the same distance. This "pressure well" is theoretically the maximum pulling force per unit area which has to be applied in order to separate the two surfaces. In fact, highly attractive conditions (pressure well deeper than ~ -40 MPa) were obtained in a broad range of charge densities, from about -2 to -3.5 e/nm^2. The corresponding distances for maximum attraction went from about 0.7 to 1 nm, but significant attractive pressures (say, larger than 1 MPa) are already detected at 2 nm. At still higher charge densities, repulsive contact interactions in the crowded interlayer space start to compensate the electrostatic attraction. A summary pressure versus distance map is shown in Fig. 8.

These calculations were revisited by Jönsson et al. [37,38] both in the canonical and the grand canonical ensemble, that is, by imposing the chemical potential of ions rather than their number. This allowed them to calculate, among other features, the influence of added electrolytes and the apparent surface charge. A main result is the remarkably robust character of the attractive conditions at high surface charge densities, even in the presence – like in real cement – of high monovalent ions concentrations. Another important result is the good agreement between the calculated pressure versus distance curves and the experimenttal force versus distance curves obtained by AFM measurements between a C–S–H covered tip and a C–S–H covered single crystal calcite surface (based on a reasonable hypothesis for the effective interaction area in the tip-substrate gap) [39,40].

4. Cohesion at sub-nano scale: The atomistic approach

The results summarized in the previous section show unambiguously that ionic correlation forces contribute significantly to the overall cohesion of C–S–H. However, rigorously speaking, this conclusion should be restricted to those parts of the microstructure where the very conditions for the occurrence of

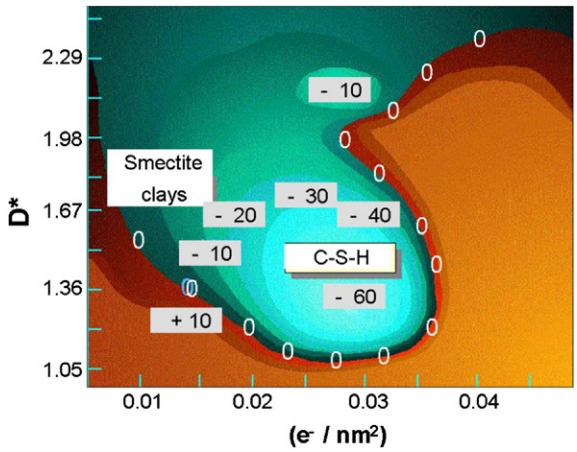

Fig. 8. Isobaric contour map for the interaction between two negatively charged surfaces facing each other, with calcium counterions in water. Positive and negative pressure values (in atm, or 10^5 Pa) correspond to repulsive and attractive situations, respectively. The surface charge density (abscissa scale) for a fully ionized C–S–H surface (3 e^-/nm^2) corresponds to the deepest attractive pressure well. The separation distance $D^*=D/d$ (vertical scale) is expressed in units of hydrated calcium ion diameters, d. The zero pressure line is the locus of equilibrium positions (adapted from [36]).

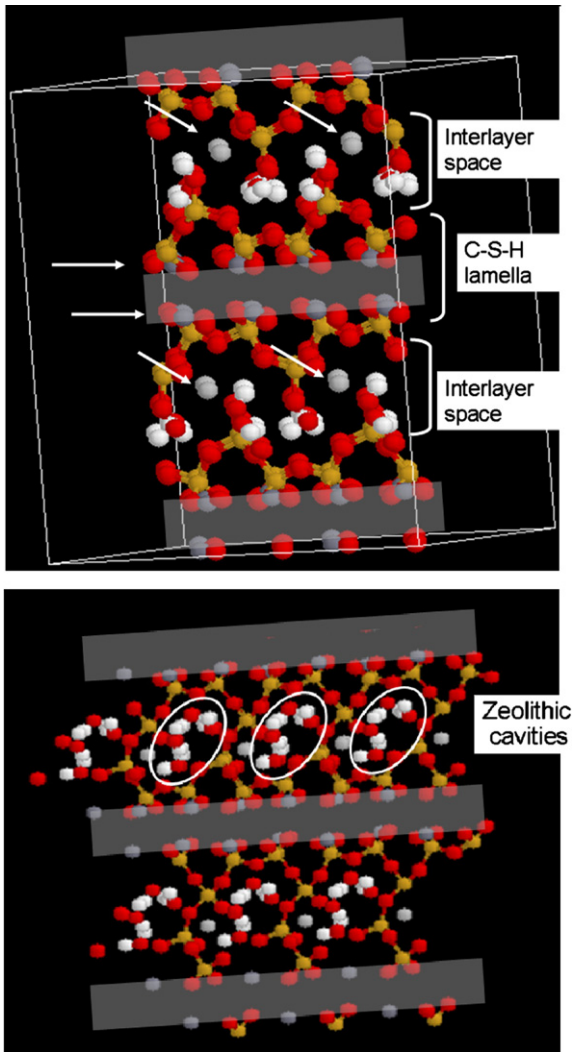

Fig. 9. A relaxed configuration of tobermorite-like C–S–H (starting from Hamid's structure of 11 Å tobermorite) after potential energy minimization, at Ca/Si=0.83 and 4 water molecules per unit cell in the interlamellar space. The hydrogen atoms are in white. The interlamellar calcium ions are in light grey and pointed by the tilted arrows. The calcium ions of the Ca–O backbone are in dark grey and pointed by horizontal arrows.

ionic correlations are met. Those conditions are also the conditions for the validity of the Monte Carlo simulations which were achieved in the primitive model framework: homogeneously charged surfaces, mobile ions, in a dielectric continuum. As already discussed in Section 2.1, this is a set of conditions which is acceptable when the distance between C–S–H lamellae (either isolated lamellae, or the outer lamellae of a particle) is larger than, say, a few hydrated calcium ion radii. In this respect, the distance at which the maximum attractive pressure is obtained in the simulations is at the limit of what is acceptable since it corresponds to only two or three times the diameter of a water molecule, or less. This shed some doubt on the accuracy of the primitive model approach in these conditions. At the least, the molecular structure of water should be taken into account. The possible loss of mobility of the ions in such confined conditions and the localization of the surface charges in the C–S–H lamellae are other reasons to switch to an atomistic description. In this section we review the results obtained by using tobermorite as the starting atomic scale model for C–S–H structure, on the interactions between tobermorite lamellae in very confined geometries. Such confined conditions would correspond to neighboring lamellae within a particle, or to "contact" spots between particles.

Atomistic level simulations have been only scarcely applied to the structure and cohesive properties of C–S–H so far [36,41–46]. Using *ab initio* modeling at the Hartree–Fock level (that is, resolving Schrödinger equation), Manzano et al. [43] studied the formation of tobermorite-like and jennite-like dimeric units (T_2 and J_2, respectively), starting from a single precursor structure composed of two silicate dimers and a single oxide layer. They showed that, indeed, depending on the Ca/Si ratio, T_2 or J_2 were obtained. Interestingly, T_2 dimers have a very small dipole moment (3.4 or 1.7 Debyes, depending on the number of water molecules coordinated to the structure) whereas J_2 dimers have a very large one ($\geq$25 Debyes). Since a high dipole moment favors the formation of larger structures by dipole–dipole interactions, this might be a clue to understand the difference between the large persistence length of the outer product as compared to the inner product (see Section 2.1, [2]).

The previous approach, in which the material is constructed from atoms or small building blocks without any *a priori* on the obtained structure, would be the most powerful to study the cohesion of C–S–H. However, it is also very demanding computer-wise. An alternative approach is to start from a crystalline structure which is already a reasonably good approximation of the real structure. This is the method which has been used by Gmira et al. [44–46]. Starting from the atomistically resolved structure of the so-called 11 Å tobermorite, either that proposed by Hamid [47] or that proposed by Merlino et al. [48,49], three numerical methods were used: (i) potential energy minimization using empirical interatomic

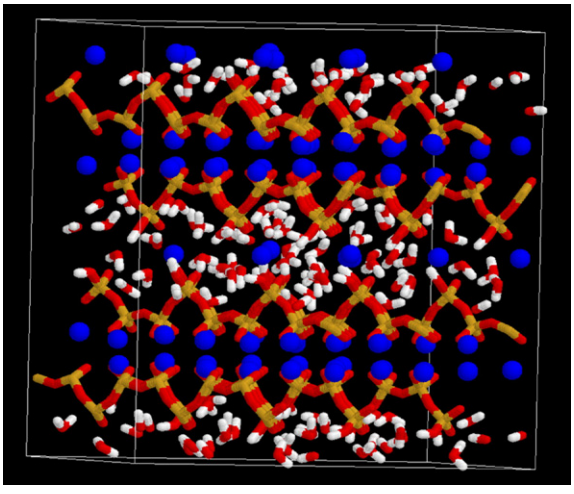

Fig. 10. A relaxed configuration of tobermorite-like C–S–H (starting from Merlino's structure of 14 Å tobermorite, which has no Si–O–Si interlamellar bridges) after potential energy minimization, at Ca/Si=0.83 and 14 water molecules per unit cell in the interlamellar space. Calcium ions are in blue and water molecules are the red (oxygen) and white (hydrogen) objects. (For interpretation of the references to colour in this figure legend, the reader is referred to the web version of this article.)

Table 1
Energy minimization results (unit cell parameters; bond lengths and angles) at 0 K for 11 Å tobermorite in Hamid's model at Ca/Si=1.0, $4H_2O$/unit cell, and Ca/Si=0.83, $4H_2O$/unit cell

	a (Å)	b (Å)	c (Å)	α (°)	β (°)	γ (°)	Ca0 (Å)	SiO (Å)	O–Si–O (°)
Model	7.39	22.78	6.69	90.00	123.49	90.00	2.35–2.75	1.55–1.67	–
Simul. 1.0	7.30	24.50	6.65	90.28	123.75	89.93	2.35–2.67	1.49–1.67	100.61–119.35
Simul. 0.83	7.38	23.26	6.75	90.00	123.28	90.00	–	–	–

potentials, in order to calculate thermodynamic and elastic properties; (ii) periodic *ab initio* quantum calculations on the energy minimized structure in order to obtain the cohesion energy and the bonding scheme; (iii) molecular dynamics of the interlayer calcium ions and water molecules in order to obtain their self-diffusion coefficient. More technical details of these methods are given in the Appendix.

Tobermorite polytypes may be classified on the basis if their basal spacing (14, 11 or 9.3 Å), which is related to their water content. The 14 Å tobermorite transforms to the 11 Å form by heating from 60 to 100 °C. Subsequent heating to 300 °C for a few hours gives rise to the 9.3 Å tobermorite. Two atomistically resolved structures of 11 Å tobermorite – one due to Hamid and another due to Merlino et al. – are available in the literature. Both are based on a composite layer of distorted central Ca–O slab that is ribbed on either side with infinite dreierketten, i.e. silicate chains that repeat at an interval of three silicate tetrahedra. Two adjacent tetrahedra forming a so-called dimer coordinate through oxygens to in-layer calcium ions while the third, pointing away from the Ca–O slab and called a bridging tetrahedron, links two successive dimers. In perfect tobermorite, at Ca/Si=0.66, all the oxygen atoms involved in the dangling bonds of the silicate chains are protonated as hydroxyl groups and the structure is neutral. The interlamellar space contains only water molecules. At higher Ca/Si ratio, the OH groups are ionized and the hydrogen ions are replaced by calcium ions in the interlamellar space. Their amount depends directly on the number of layer OH groups that in turn depends on pH. In Hamid's model the layers are not chemically bonded to each other. The main difference introduced in Merlino's model compared to the independent layer model of Hamid consists is the presence of Wollastonite chains (linked silicate tetrahedra between facing silicate chains). These layer-to-layer Si–O–Si chemical linkages induce the formation of cavities similar to those present in zeolites. They do not exist in the 14 Å form. Relaxed (that is, after potential energy minimization) configurations of Hamid's and Merlino's 11 Å tobermorite-like C–S–H are shown in Fig. 9. A more hydrated 14 Å form is shown in Fig. 10.

Qualitatively, a first important point coming out of the relaxed structures is that the interlamellar calcium ions are not randomly distributed. They occupy well defined sites, either directly close to an oxygen atom or with a water molecule in between. This is a first indication that concentration fluctuations and correlation forces can hardly be considered within such narrow gaps.

Globally, the structural results of the energy minimization procedure are in better agreement with Hamid's structure than with Merlino's structure. As shown in Tables 1 and 2 for 11 Å tobermorite with Ca/Si=0.83 or 1.0 and $4H_2O$ per unit cell, this is particularly noticeable when one looks at unit cell angles. The difference between experimental (i.e. refined from X-ray diffraction) and simulated unit cell parameters is less than 3% for the structure proposed by Hamid and 12% for the characteristic angles in Merlino's structure.

As far as stability is concerned, the results of the potential energy minimization method are less conclusive. The most physically sound comparison method is based on the energy density, i.e. the potential energy of the unit cell after relaxation divided by the unit cell volume. The energy densities calculated at the minimum of the energy versus separation distance curve for Hamid's and Merlino's structures at Ca/Si=1 (Table 1) are −2.07 and −2.15 eV/Å^3, respectively. Considering the flatness of the potential energy curve in the region of the deepest minimum (Fig. 11), this is not significant. In contrast, the 8% difference in potential energy calculated by the *ab initio* method, in favor of Hamid's structure (−0.41 and −0.38 eV/Å^3, respectively, at Ca/Si=0.83), is significant, thanks to the intrinsically higher quality of the *ab initio* calculations (only the comparison of values obtained by a given numerical method is meaningful). The reason for this slightly higher stability of the "independent" lamellae form with respect to the 3D bonded form – surprising at first sight – has to be found in the larger constraints on angles and bond lengths in the latter.

The conclusion to be drawn from the previous comparison is that, after all, fine details of the C–S–H structure do not matter that much, as far as cohesion is concerned. The electrostatic interaction between "independent" charged lamellae via the interlamellar calcium ions is virtually as strong as a Si–O–Si chemical bond. This conclusion is confirmed by the Mulliken electronic charges obtained from the *ab initio* simulation (Table 3). The ratio between Mulliken and formal charges quantifies the ionic character of the bonds. In the case of tobermorite-like C–S–H, it is found that the ionic character of

Table 2
Energy minimization results (unit cell parameters; bond lengths and angles) at 0 K for 11 Å tobermorite in Merlino's model (Ca/Si=0.83, $4H_2O$/unit cell)

	a (Å)	b (Å)	c (Å)	α (°)	β (°)	γ (°)	Ca0 (Å)	SiO (Å)	O–Si–O (°)
Exp.	11.92	11.92	6.732	80.26	99.73	35.99	2.28–2.61	1.60–1.68	–
Sim.	12.61	11.75	6.713	98.61	107.20	35.66	2.22–2.43	1.54–1.66	98.81–124.20

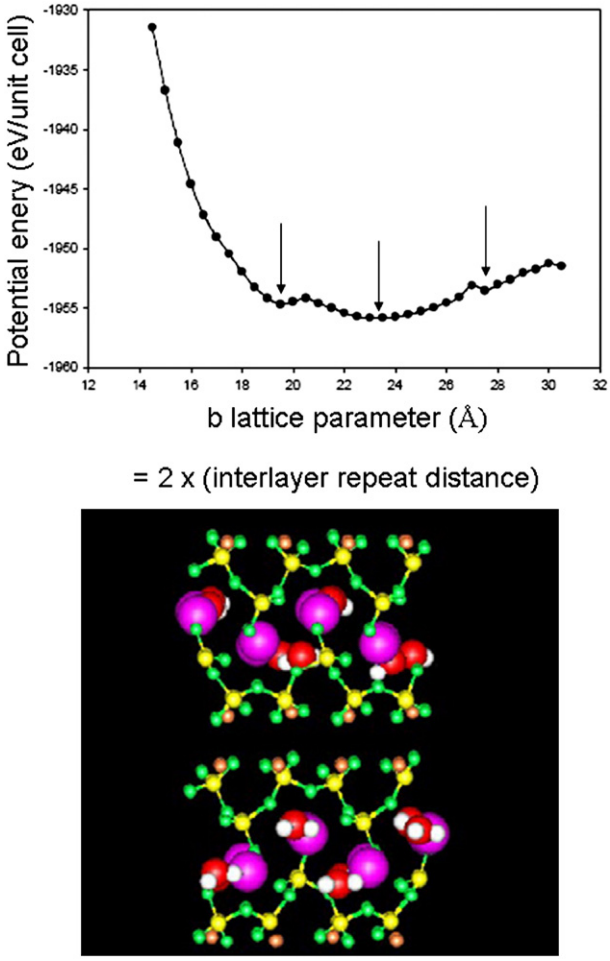

Fig. 11. Top: potential energy (at 0 K) as a function of the *b* lattice parameter for tobermorite-like C–S–H at Ca/Si = 0.83 and 4 H_2O/unit cell (Hamid's structure). The three minima correspond quite well to the so-called, 9, 11 and 14 Å structures, respectively. The stable minimum is the 11 Å structure. Bottom: snapshot of the simulated system for molecular dynamics calculation of the water self-diffusion coefficient.

the intra-lamellar bonds is close to 60% on average, which implies that the covalent character is close to 40%. This is not surprising for a divalent silicate. More interesting is the charge on the interlamellar calcium ions (+1.38), which is only slightly larger than the charge on the calcium ions within the lamellae (+1.29) and still far from the value expected for a free calcium ion (+2). Furthermore, the distance between the interlamellar calcium ions and the oxygen ions of the closest lamella is very close to the Ca–O distance within the lamellae. Together with the Mulliken charge, this is the clear signature of a chemical bond and may be considered as the reason for the non-exchangeable character of these ions, contrary to the mobile and exchangeable character of interlamellar ions in smectite clays. Interestingly, Mulliken charges, including that of the interlamellar calcium ions, do not change when varying the interlamellar distance from 0.75 to 1.6 nm. This means that the nature of the interlamellar bonding remains unchanged and is therefore essentially electrostatic.

The results of the molecular dynamics simulations performed on the water molecules, at 300K and fixed interlamellar separation (Ca/Si = 1 and 4 H_2O/unit cell) over 131 ps led to a self-diffusion coefficient of the order of 3.4 10^{-12} m^2 s^{-1}. This figure is about 1000 times smaller than the value obtained for bulk water (4.1 10^{-9} m^2 s^{-1}, as compared to 2.3 10^{-9} m^2 s^{-1} for the experimental value). The molecules are essentially wobbling around their equilibrium positions, trapped by the interlamellar calcium ions (Fig. 11). This confirms that all interlamellar species in such confined conditions are strongly localized in rather well defined crystallographic sites.

Returning to the energy versus interlamellar separation curves for Hamid's structure obtained by the classical energy minimization method, it is interesting to see that several minima are obtained at 1.1, 1.225 and 1.4 nm, respectively (Fig. 11), the latter being less stable than the oithers, in agreement with the experimental observation that dehydration of the 1.4 nm form is irreversible [3]. The free energy curve at 300 K has basically the same shape as the 0 K curve. The gap between the two curves remains constant at large distance but diminishes slightly at short distance due to the vibrational entropy effect in this domain. The cohesion energy curve obtained from the *ab initio* method is very close to that obtained by potential energy minimization, but the two first minima merge into a single one at 1.2 nm [46].

The simplest way to compare the results of the atomistic approach for confined conditions with the primitive model approach for less confined conditions is to compare the pressure versus interlamellar separation curves. Such a curve is the first derivative of the free energy versus separation curve (Fig. 11). The result is shown in Fig. 12, together with the curve derived from the primitive model in the most attractive conditions (this is a vertical section in Fig. 8 at a surface charge density of 0.03 e^-/nm^2. It should be realized that in such a representation, the equilibrium positions of the lamellae correspond to the zero pressure positions. As far as cohesion is concerned, the most important property is the value of the largest attractive (i.e., negative) pressure which has to be overcome in order to separate the lamellae at infinite distance from each other. This value is ~5 GPa in the confined conditions considered in the atomistic approach and only ~0.6 GPa in the less confined conditions modelled by the primitive model.

The cohesive pressure is not the only parameter which can be calculated from the potential energy minimization. All elastic properties can be estimated from the relaxed configurations, including the density of vibrational states (the IR spectrum) [44]. Table 4 summarizes the modulus (bulk, shear, Young's's) values calculated from the elastic and compliance matrices of elastic coefficients, respectively (also known as Voigt and Reuss moduli), as described in detail elsewhere [50]. For the 1.2 nm (repeat distance) form at Ca/Si = 1 and 4 water molecules per unit

Table 3
Ab initio Mulliken charges in Hamid's model of tobermorite

	Si	Ca_{layer}	Ca_{inter}	O_{layer}	O_{water}	H_{water}
Q(e^-)	+2.39	+1.29	+1.38	−1.23	−0.42	+0.21
	(+4)	(+2)	(+2)	(−2)	(−2)	(+1)

Also indicated are the formal charges.

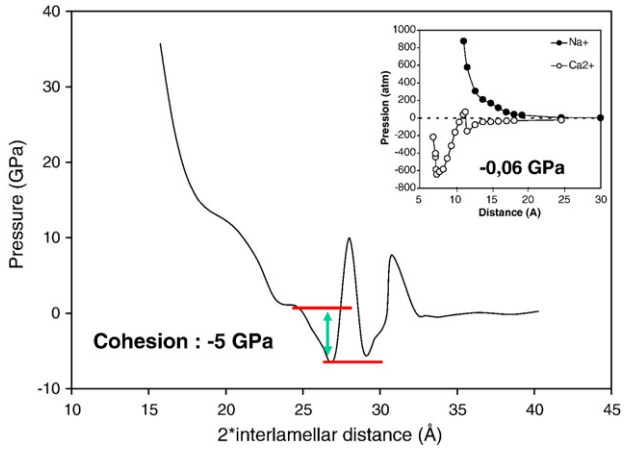

Fig. 12. Interlayer pressure versus distance plot for tobermorite-like C–S–H at Ca/Si=0.83, 4 H_2O/unit cell (Hamid's structure). Positive and negative values correspond to repulsive and attractive pressures, respectively. Inset: interlayer pressure against distance curve calculated by Monte Carlo in the framework of the primitive model, for two flat surfaces with a surface charge density corresponding to a fully ionized tobermorite surface [32]. The upper (repulsive) and lower (mainly attractive) curves are for Na and Ca interlayer ions, respectively. The cohesion pressure, that is, the largest attractive pressure to overcome in order to break the "bond" is 5 GPa in the atomic simulation and only 0.6 GPa in the primitive model calculation. Note that the distances in the main figure and in the inset are not directly comparable. In the inset, it is the true gap between the two surfaces, but those surfaces have no atomic structure. In the main figure, it is twice the repeat distance of the true atomic structure along the direction perpendicular to the lamellae. In order to obtain the interlayer distance, the lamellae thickness should be substracted twice from those values, but this is a risky operation, due to the complex surface topography of a tobermorite lamella.

cell, all modulus values are in the tens of GPa range. The average Young's modulus $\langle E \rangle$ (averaged over $E_{//}$ and $E_{\perp}$ in the parallel and perpendicular directions with respect to the lamellae plane, respectively) is 89 GPa. At Ca/Si=0.83, the shear moduli and the Young's modulus are smaller ($\langle E \rangle$=63.5 GPa). As expected, the shear modulus for shear along the interlamellar plane is smaller than the bulk modulus, and the Young's modulus along the stacking direction is much smaller than in the transverse directions. The later difference is undoubtedly due to the nanoporous character of the interlamellar space.

In general, ignoring elastic anisotropy, elastic moduli are often expected to be proportional to density if the bond strengths are similar. Thus, it is interesting to see how the moduli of tobermorite-like C–S–H follow this trend together with different forms of silica, alumina, magnesia and their compounds, including clays and zeolites. The Young's moduli of twenty-three compounds are plotted against their density in Fig. 13. As shown by Chen and Evans [51], the polymorphs of silica and alumina increase smoothly with density with a linear fitting of the form $E(\mathrm{GPa}) = -377 + 0.189\rho$, where the density ρ, ranging from 2200 to almost 4500, is expressed in kg m^{-3}. The same authors also showed that within standard deviation this curve passes also through the data points for mullite ($3Al_2O_3.2SiO_2$), sillimanite ($Al_2O_3.SiO_2$), $2Al_2O_3.SiO_2$, muscovite mica and montmorillonite clays. For the montmorillonite clay, the modulus which was taken into account is that of a single clay lamella (thus, no interference with the interlamellar space).

In order to strengthen the correlation, one more literature data point for kaolinite [53] and ten calculated values, including values for quartz, cristoballite, corundum alumina, MgO, pyrophyllite, antigorite, lizardite, chabazite, silicalite and faujasite, obtained by the potential energy minimization method [52], have been added in Fig. 12. Except for the zeolites, which are highly porous, the correlation holds. The modulus of zeolites is somewhat larger than predicted from the linear E versus ρ correlation. This is not surprising: the linear relationship of Chen and Evans is necessarily a strong approximation since it predicts a vanishing modulus for silicates with a density below 2 kg m^{-3}. Remarkably, the values calculated for tobermorite-like C–S–H fall well within the general correlation. The remarkable feature is that, in the case of tobermorite, the modulus is that of a stack of lamellae *including the interlamellar species*. Thus, what this result is telling us is that a stack of C–S–H lamellae in its stable configuration has to be considered as a continuous construction of ionic-covalent bonds, not basically different in nature from a crystal of quartz or alumina. This strong result has far-reaching consequences.

5. Ionic-covalent bonds versus ion correlation forces. Prospects for improvement

Strictly considered, the results discussed in the two previous sections refer to the interactions of two C–S–H lamellae or their model. These lamellae may be isolated lamellae or the surface lamellae of particles containing several lamellae. Within the approximations which have been made in building the models, it does not make any difference. The results show that short- and medium-range attractive electrostatic forces are the essential components of the cohesion of C–S–H. At short, sub-nm, distances (distances corresponding to one or two water molecule

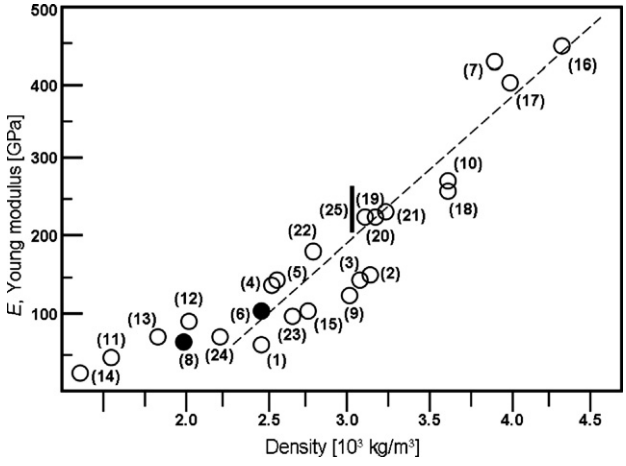

Fig. 13. Correlation between density and Young modulus for quartz (1), dehydrated pyrophyllite at 0 GPa (2), dehydrated pyrophyllite at 10 GPa (3), antogorite (4), lizardite (5), tobermorite-1.2 nm (6), corundum alumina (7), tobermorite-1.4 nm (8), swollen and dehydrated pyrophyllite (9), MgO (10), chabazite (11), cristoballite (12), silicalite (13), faujasite (14), kaolinite (15), stishovite (16) alumina (17), alumina (18), $3Al_2O_3.2SiO_2$ (19), $Al_2O_3.SiO_2$ (20), $2Al_2O_3.SiO_2$ (21), muscovite mica (22), fused silica (23). Data points (1) to (14) were obtained by energy minimization [52]; data (15) is from [53]; data points (16) to (24) and bar for clays (25) are from [51].

diameters), the C–S–H lamellae are trapped into an extremely deep potential well, in a configuration involving quasi-immobile interlamellar water molecules and calcium ions which are bonded to the closest lamella by a partly covalent bond. At larger (a few nm) distances, the lamellae or stacks of lamellae are trapped in less deep potential wells generated by ionic correlation forces involving mobile ions in liquid water films.

It is difficult to establish *a priori* the respective contribution of these two types of forces without having a *very* detailed model for the fabric of the C–S–H lamellae in a "mechanically representative volume", which may be orders of magnitude larger than a single lamella. There is little doubt that within the locally ordered stacks the ionic-covalent forces are dominating. The same holds for the spots where two stacks come in "contact". However, the structural conditions for having this very strong interaction are very stringent. The ion correlation forces are weaker but they require much less stringent structural conditions. Considering the very disordered character of the C–S–H "gel" in a dense cement paste, it is likely that these forces generate a kind of background attractive pressure contributing significantly to the overall cohesion.

Several arguments point towards the prevalent role of the iono-covalent bonds. The first and strongest argument is the good, order-of-magnitude (or better), agreement between the calculated and experimentally measured moduli. High quality and statistically significant measures of the indentation modulus of C–S–H in hardened cement pastes by the so-called "grid nanoindentation technique" have been performed in recent years [54–56]. The indentation modulus M is related to the Young's (E), shear (G) and bulk (K) moduli and to the Poisson ratio (ν) by simple relationships [57]:

$$M = \frac{E}{1-\nu^2} = 4G\frac{3K+G}{3K+4G} \tag{2}$$

With usual values of ν (~0.25), it is easy to see that M is only slightly larger (~10%) than E. Most measured values fall between 10 and 40 GPa, with several frequency peaks. The main frequency peaks appear around 20 and 30 GPa, respectively. They were interpreted in terms of the nanogranular model of C–S–H proposed by Jennings [58,59], in which two types of C–S–H – low density (LD) and high density (HD) C–S–H – are considered in order to account for the evolution of surface area, density and porosity with degree of hydration. Both LD and HD C–S–H are made of the same, almost compact (11% porosity), nanosized building blocks (4 to 5 nm), but they differ by their aggregation density. Thus, the 20 GPa peak was assigned to low density C–S–H and the 30 GPa peak was assigned to the high density form. Lower values were interpreted in terms of interference with the capillary porosity.

AFM has also been used to measure the indentation modulus of atomically smooth C–S–H particles grown on single crystal calcite surfaces [60]. The thickness of the particles was of the order of several hundreds of nm and, after careful re-crystallisation, their lateral extension reached ~1 μm. In these conditions, AFM provides high quality measurements. Furthermore, the Ca/Si ratio in the C–S–H was modulated by equilibration with lime solutions of different concentrations, from 0.16 to 19.13 mmol/L. Besides increasing the Ca/Si ratio, this also regulates the interlamellar repeat distance, from 1.4 nm at low lime concentration to 1.2 nm as saturation is approached. The Young's modulus was found to increase from ~120 GPa at low lime concentration to ~300 GPa at high lime concentration when the Ca/Si ratio is approaching 1.5. These values are considerably larger than those reported above, which were obtained with a more classical nanoindenter instrument [54–56]. However, as noticed by the authors of the AFM measurements [60], the AFM measurements were performed on what may be considered as an oriented single crystal of C–S–H, whereas the grid nanoindentation results refer to disordered packings of nanocrystalline particles, with some packing porosity. Another difference which may be mentioned, and which has probably even larger consequences than the presence of some nanoporosity, is the orientational averaging in the grid nanoindentation measurements.

The Young's modulus values obtained by atomic scale simulation in the direction perpendicular to the lamellae plane, $E_\perp$, compare quite well with those which were experimentally measured by AFM at low lime concentration and low Ca/Si ratio. Interestingly, the increase of $E_\perp$ when Ca/Si increases is observed both in the simulations and in the measurements. On the other hand, the comparison between the simulations and the grid nanoindentation results [54–56] is best made by comparing the experimental values (20 and 30 GPa for LD and HD C–S–H, respectively) with the calculated $\langle E \rangle$ (Table 4). The calculated values are ~2–3 times larger than the measured values. As mentioned above, this is not unexpected, considering the imperfect packing of the nanoparticles in the LD and HD aggregates. As a matter of fact, the surprising feature is that, *in spite* of this imperfect packing, the measured values are *only* 2 or 3 times smaller than the calculated values. This has a profound significance. It means that the elastic properties of a unit composed of two C–S–H lamellae in iono-covalent interaction in very confined configuration are basically comparable to those of much larger aggregates. Or stated differently: the forces which hold the nanoparticles together in the LD and HD aggregates are basically similar to the forces which hold the lamellae together within a nanocrystalline particle.

Table 4
Elastic parameters of two tobermorite-like C–S–H structures calculated by the classical potential energy minimization method

	Ca/Si=0.83 1.4 nm	Ca/Si=1 1.2 nm
K_{Voigt}	35.4 GPa	61.9 GPa
K_{Reuss}	20.7 GPa	53.8 GPa
G_{Voigt}	5.08 GPa	32.2 GPa
G_{Reuss}	2.78 GPa	23.2 GPa
ν_{Voigt}	0.25	0.25
ν_{Reuss}	0.26	0.26
$E_{//}$	94–91 GPa	91 – 113 GPa
$E_\perp$	5 GPa	61.5 GPa
$\langle E \rangle$	63.5 GPa	89 GPa

Middle column: Ca/Si=0.83, $4H_2O$/unit cell, 1.4 nm interlamellar repeat distance. Right column: Ca/Si=1, $4H_2O$/unit cell, 1.2 nm interlamellar repeat distance. K: bulk modulus; G: shear modulus; E: Young's modulus; ν: Poisson ratio.

A second argument pointing to the primary role of iono-covalent forces and the secondary role of the ion correlation forces in the upscaling process towards macroscopic properties is the creep behaviour of C–S–H. Cement pastes do not creep extensively. Creep is virtually non-existent in dry pastes and is only very limited in water-saturated pastes, with kinetics which decrease logarithmically with time [54]. Ion correlation forces between parallel surfaces are not expected to withstand shear forces [61]. They are invariant as far as translation of one surface with respect to the other is concerned. Thus, if ion correlation forces were the most important cohesive forces, creep would most probably be much more extensive than it actually is. However, it should be recognized that this argument does not take into account the possible creep-limiting role of "dry" friction, which may restrict creep in a randomly oriented populations of lamellae, just like dislocation crowding limits the plastic behavior of metals.

The third argument in favor of the key role of very short-range iono-covalent bonds in macroscopic behavior is the observation commented by Powers in an illuminating discussion of the source of cohesion in C–S–H [62]. As pointed out by Powers, "*…converting* [C–S–H] *gel to well-organized crystals by curing in steam of about 400°F destroys cohesion*". This strongly supports an overall picture in which the source of cohesion has to be looked for in the contact zones between C–S–H nanoparticles. Indeed, there is no reason for which cohesion due to ion correlation forces would decrease when the size of the interacting surfaces increases. On the contrary, a decrease of cohesion with particle size is exactly the expected behavior for any cohesion mechanism involving forces acting at contact spots (for instance, with spherical particles of radius R in random packing, the number of contact spots per unit area of cross-sectional plane is scaling as R^{-2}).

At this point, the obvious question is: what can we do or what should be done in order to improve the macroscopic cohesion of C–S–H? The first and most obvious route would be to tune the parameters which control the cohesion forces. To increase the charge density on the C–S–H lamellae and/or to increase the charge of the interlamellar ions while simultaneously decreasing their size would be beneficial both for ion correlation forces and for by iono-covalent interactions. The main problem is that it is notoriously difficult to dope the C–S–H lamellae and to ion-exchange the interlamellar ions. Nevertheless, the significant differences in elastic properties which were obtained from the simulations simply by changing the Ca/Si ratio from 0.83 to 1 and the stacking repeat distance from 1.4 to 1.2 nm (Section 4, Table 4), confirmed by AFM measurements, show that there is room for tuning.

A different and probably more open route would be to try to control the microstructure in such a way as to optimize the surface area on which the cohesion forces are acting. Based on the conclusion that we reached so far, that is, that strong iono-covalent "contact" or "surface" forces are the main source of cohesion, the best option would be to try to orient and limit the lateral growth of the C–S–H lamellae in order to ultimately form the largest possible dense assemblies of small and compact nanoparticles like in the high density model of C–S–H proposed by Jennings [58,59]. However, though favorable to the ultimate strength in aged samples, this option would probably be not the best one in order to favor early age strength development. Aggregation of the particles in long fibrils would be more beneficial for that purpose. In this respect, it would be of great interest to understand better the interactions which lead to the widespread liquid crystal-type of order which is observed in the outer product and also, to a lesser extent, in the inner product.

A totally different option, inspired from the microstructure of smectite clays, would be to favor lateral growth and to limit strongly the thickness of the ordered stacks in order to favor entanglement, like in Fig. 6. This would generate large contact areas and promote structural continuity, thanks to the increased deformability of the stacks. This is not unrealistic. The elastic modulus of a single montmorillonite lamella is higher than that of a C–S–H lamella. Yet, thanks to their large lateral extension, even relatively thick stacks of montmorillonite lamellae are able to adopt rather short curvature radii (Fig. 6). The strongest microstructure along this line would be a dense entanglement of flexible individual lamellae. This is supported by tensile strength measurements on thin self-supporting deposits of montmorillonite, cation-exchanged with different ions [63]. Interestingly, the strongest samples were those with well hydrated monovalent ions whereas the weakest samples are those exchanged with divalent or trivalent ion. In spite of their stronger and thicker nanocrystalline particles, the latter samples are macroscopically weaker due to the lower deformability of the stacks which prevents entanglement and limits the bonding continuity to tiny contact spots.

6. Towards hybrid hydrates

There are several ways to synthesize C–S–H. The most important in practice is for obvious reasons the hydration of C_3S. Alternative routes may involve the so-called pozzolanic reaction between reactive silica and a lime solution, or the direct precipitation from a solution containing silicate ions and lime at high pH. It has recently been shown that co-precipitation of a mixture of organotrialkoxysilane, tetraethoxysilane (TEOS) and a calcium salt in aqueous/ethanolic basic solution leads to a variety of solids including neat C–S–H, a layered calcium organosilicate hybrid with a clay-like structure [64], or truly hybrid C–S–H with varying amounts of organic groups in the interlayer space, directly linked to the silicate chains [65].

In the absence of organotrialkoxysilane (that is, using only TEOS), a relatively well crystallized C–S–H is obtained. In the opposite case; hydrolysis with 100% organotrialkoxysilane leads to a layered calcium alkyl-silicate in which the silica tetrahedra are forming a continuous layer on each side of a central brucite-like calcium octahedral layer. The alkyl chains, covalently bonded to the silica sheets, are forming a bilayer in the interlayer space (Fig. 14). As expected, the basal distance is increasing linearly with the length of the alkyl chains.

The most interesting materials as far as cementitious binders are concerned are those obtained at intermediate substitutions of TEOS by the organotrialkoxysilane. The structural data obtained

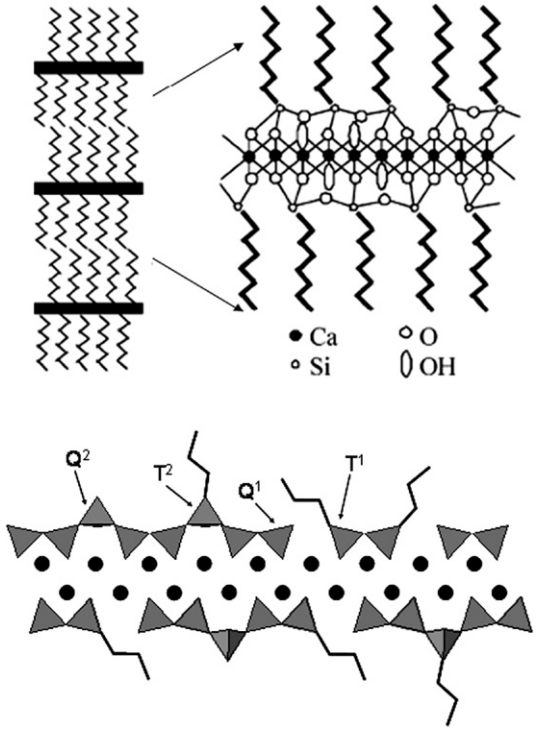

Fig. 14. Top: Structure of the clay-like layered calcium alkyl-silicates obtained by hydrolysis of organotrialkoxysilane. The central sheet has a brucite-like structure and the silica tetrahedral form a continuous 2D structure like in smectite clays (adapted from [64]). Bottom: Schematic model of a layer of hybrid calcium-silicate materials showing the incorporation of organotriethoxysilane at the end and in the middle of silicate chains of C–S–H. The various ^{29}Si NMR species are also shown. (● = calcium atoms) (Adapted from [65]).

by X-ray diffraction and by 1D and 2D solid-state NMR show that the silica tetrahedra recover the chain structure typical of C–S–H and that the organic groups are covalently bonded to the inorganic framework (Fig. 14). This was achieved with short organic chains (ethyl, *n*-butyl or 3-aminopropyl) with poor mechanical benefit, but very positive results have recently been obtained by reaction of silylated polymers with OPC pastes [66]. The polymers were copolymers of polydimethylacrylamide and poly(butadiene-*g*-oxyethylene) silylated with T-silanes. ^{29}Si–^{1}H CP NMR in deuterated solvent shows the close proximity of the silane with the C–S–H backbone. Only T-silanes were able to link to the C–S–H. Remarkable mechanical improvements were observed. Young's modulus enhancements between 40 and 100% were obtained with as little as 0.5% polymer (w/w) with respect to cement. ^{1}H NMR relaxation shows that the polymer remains in a mobile state after reaction. This means that the modulus increase can in no way be explained in terms of a mixture model since the added material is softer than the mineral matrix. Among the possible explanations, the most likely is the influence of the polymer on the nucleation and growth of the C–S–H and possibly on the connectivity of the matrix.

7. Conclusions

The atomic scale calculations reported in this paper show that when two parallel tobermorite-like C–S–H lamellae (or stacks of lamellae) at low Ca/Si ratio are at a distance of the order of one or two water molecular diameter (the 1.2 nm repeat distance form), they are trapped in an extremely deep electrostatic potential well which may be considered as a chemical ionic bond. No interlamellar bridging by silica tetrahedra is needed for this. Addition of water is not able to extract the lamellae from their well. Furthermore, the bond between the interlamellar calcium ions and the lamella to which they are closest has a significant covalent character. This is related to the incomplete hydration of these ions and explains their essentially non-exchangeable character. The interlamellar calcium ions are not in a symmetric bridging configuration: they are close to a lattice oxygen atom on one side and close to an oxygen atom of a water molecule on the other side. The water molecules themselves may be considered as highly localized since their diffusion coefficient obtained by molecular dynamics shows that they are diffusing about a thousand times slower than in bulk water at the same temperature.

On the other hand, Monte Carlo simulations in the framework of the primitive model show also that when two lamellae (or stacks of lamellae) are separated by a distance large enough to allow for full hydration and mobility of the calcium ions, strongly attractive correlation forces may appear, leading to cohesive behavior at larger equilibrium distances. This is in agreement with direct force measurements by AFM.

The comparison between the moduli experimentally measured on cement paste and on single crystalline C–S–H surfaces, and the moduli of C–S–H assemblages calculated by atomic scale simulation, show that the C–S–H matrix has to be considered as a lacunar iono-covalent (in the sense explained in the first paragraph of the Conclusion) continuum. The C–S–H matrix owes its stiffness essentially to the very short-range electrostatic forces at contact spots between nanoscale lamellae stacks. This is further confirmed by the creep behavior of C–S–H and the particle size dependence of strength.

Based on the previous conclusions, two approaches have been explored, which may ultimately open new ways for improving the mechanical performances of cementitious materials, either at early age or in mature materials. One is based on the engineering of the bonding scheme which ensures the cohesion of the C–S–H matrix, either by increasing the strength of the iono-covalent and the ion correlation "bonds", or by modifying the microstructure in such a way as to optimize connectivity. Among the two routes, the second seems the most realistic, but its implementation would require serious progress in our understanding of C–S–H growth and aggregation. In particular, the strong tendency of C–S–H units to form oriented aggregates has to be understood. Another, bioinspired, approach is based on the covalent hybridization of the hydrates with small organic groups or with polymeric chains. Recent results obtained with silylated polymers show that minute degrees of hybridization are able to generate a strong improvement in mechanical properties. Once more, a deeper insight of the influence of organic additives on C–S–H growth and aggregation is needed. When taken together, these two strategies could form the basis for what would be a truly nanotechnological roadmap for cementitious construction materials. Molecular simulation methods and the modelling of microstructure-mechanical properties relationships, at all length scales, have a key role to play in this quest [67].

Appendix A. Numerical methods

Energy minimization

0 K energy minimization was performed using the General Utility Lattice Program (GULP) code. These calculations were performed using a set of empirical but transferable interatomic potentials calibrated on quartz and CaO. Anions (oxygen ions in tobermorite and in water) were modelled as polarizable species using the core-shell model. These transferable empirical interatomic potentials, based on the use of the formal electric charge for each interacting species, have reproduced successfully the structure and properties of many oxides [68] including silicates [69–71] and phyllosilicates [72,73] (see Ref. [74] for liquid water). They include two-body and three-body analytical functions that allow calculating the energy between pairs and triplets of atoms. They depend on the choice of some parameters that can be advantageously calibrated using *ab initio* calculations in the same simple cases. The transferability of such potential parameters in the case of more complex systems can be checked or assumed as in this work for the {Ca, Si, O, OH, H_2O} system. Note that the calculation of electrostatic interactions between pairs of ions is done with the Ewald summation scheme. The advantage of this approach compared to *ab initio* quantum mechanical methods is that one can compute for large systems with low symmetry, not only structural but also thermodynamic and elastic properties (from the elastic tensor using both Voigt and Reuss equations for bulk, shear and Young's modulus). Reference [50] gives all details on such calculations in the case of Lizardite, a magnesium silicate.

Energy minimization for finding an equilibrium structure consists in tracking stationary points that correspond to a minimum energy gradient with positive energy curvature (i.e. finding a set of atomic positions that minimizes the system energy and gives a Hessian operator with positive eigenvalues only). A phonon spectrum calculation at the center of the Brillouin zone can be used as a final validation from which one gets the list of lattice vibration frequencies that should be all positive except the three first that should be zero (unit cell translation invariance).

Such a minimization procedure gives a zero temperature solution. If one aims at calculating equilibrium properties at finite temperature, then free energy calculations are to be considered. Along with Monte Carlo or Molecular Dynamics simulations, a third possible route to study crystalline structures at a microscopic scale is thus the lattice dynamic theory. From the set of Hessian eigenvalues, one can compute the vibration partition in the harmonic approximation and deduce all thermodynamic functions including entropy and the system free energy. In the simulations discussed in this paper, energy minimization was performed using the Newton–Raphson method. All degrees of freedom were considered: atomic positions, unit cell dimensions and angles.

Periodic ab initio calculations

Ab initio methods are based on the resolution of the Schrödinger equation. In the calculations discussed in this paper, the CRYSTAL98 code for periodic system was used, using the GULP-relaxed structures (see above) as imputs. It allows calculating cohesion energy and obtaining a complete characterization of the bonding scheme in crystalline materials. Resolution of the Schrödinger equation is done using the Hartree–Fock approximation, neglecting electron fluctuations hence correlations (i.e. van der Waals dispersion forces) [75]. In this type of approach, all chemical elements in the tobermorite unit cell are described using sets of atomic orbitals. In the case of silicon and calcium, Barthelatt pseudo-potentials for core electrons were used. For hydrogen and oxygen, all electrons are considered (STO3G and 4–11G atomic basis sets, respectively) [76].

Molecular dynamics

Using the same sets of empirical interatomic potentials as in the energy minimization process, a molecular dynamics study was performed using the Nosé–Hoover thermostat. The optimized structures obtained from the energy minimization step were selected as starting configurations. The minimized cell dimensions and angles and slab species were kept fixed during the MD runs whereas the trajectories of the interlayer calcium and water species were followed. The simulations were performed at 310 K for 0.1 ns with a time step of 0.5 fs and a shell mass of 10% of the total mass of oxygen ions. The trajectories were recorded every 0.005 ps. The mean square displacements (MSD) for each interlayer species were then evaluated hence self-diffusion coefficient using the Einstein equation. The internal energy at finite temperature was calculated as the canonical ensemble average of the potential energy while the system pressure was calculated using the virial equation that requires calculating interatomic distances and resulting forces on each relaxing sites.

References

[1] I.G. Richardson, The calcium silicate hydrates, Cem. Concr. Res. 38 (2008) 137–157 (this issue).
[2] I.G. Richardson, Tobermorite/jennite and tobermorite/calcium hydroxide-based models for the structure of C–S–H: applicability to hardened pastes of tricalcium silicate, β-dicalcium silicate, Portland cement, and blends of Portland cement with blast-furnace slag, metakaolin, or silica fume, Cem. Concr. Res. 34 (2004) 1733–1777.
[3] A. Gmira, R.J.-M. Pellenq, I. Rannou, L. Duclaux, C. Clinard, T. Cacciaguerra, N. Lequeux, H. van Damme, A structural study of dehydration/rehydration of Tobermorite, a model of cement compound, in: F. Rodriguez-Reinoso, B. Mc Enaney, J. Rouquerol, K. Unger (Eds.), Studies in Surface Science and Catalysis, 144, Elsevier Science, 2002, pp. 601–607.
[4] S. Gatty, S. Bonnamy, C. Clinard, A. Feylessoufi, P. Richard, H. Van Damme, A transmission electron microscopy study of interfaces and matrix homogeneity in ultra-high-performance cement-based materials, J. Mater. Sci. 36 (2001) 4013–4026.
[5] D. Viehland, J.-F. Li, L.-J. Yuan, Z. Xu, Mesostructure of calcium silicate hydrate (C–S–H) gels in Portland cement paste: short-range ordering, nanocrystallinity, and local compositional order, J. Am. Ceram. Soc. 79 (1996) 1731–1744.
[6] X. Zhang, W. Chang, T. Zhang, C.K. Ong, Nanostructure of calcium silicate hydrate gels in cement paste, J. Am. Ceram. Soc. 83 (2000) 2600–2604.
[7] S. Gauffinet, E. Finot, A. Nonat, Observation directe de la croissance d'hydrosilicate de calcium sur des surfaces d'alite et de silice par microscopie à force atomique, C.R. Acad. Sci. Paris 327 (1998) 231–236.

[8] S. Gauffinet, E. Finot, A. Nonat, Experimental study and simulation of C–S–H nucleation and growth, in: A. Nonat (Ed.), Hydration and Setting, RILEM Pub, Cachan, 2000, pp. 199–214.
[9] S. Gauffinet-Garrault, A. Nonat, Hydrated layer formation on tricalcium and dicalcium silicate surfaces: experimental study and numerical simulations, Langmuir 17 (2001) 8131–8139.
[10] C. Plassard, E. Lesniewska, I. Pochard, A. Nonat, Investigation of the surface structure and elastic properties of calcium silicate hydrates at the nanoscale, Ultramicroscopy 100 (2004) 331–338.
[11] A. Nonat, The structure and stoichiometry of C–S–H, Cem. Concr. Res. 34 (2004) 1521–1528.
[12] R. Maggion, S. Bonnamy, P. Levitz, H. van Damme, A scaling model of the microstructural evolution in C_3S/C–S–H pastes, in: H. Jennings, J. Kropp, K. Scrivener (Eds.), The Modeling of Microstructure and its Potential for Studying Transport Properties and Durability, NATO ASI Series E: Applied Sciences, 304, Kluwer Academic Publishers, Dordrecht, 1996, pp. 137–155.
[13] I.G. Richardson, The nature of C–S–H in hardened cements, Cem. Concr. Res. 29 (1999) 1131–1147.
[14] I.G. Richardson, The nature of the hydration products in hardened cement pastes, Cem. Concr. Compos. 22 (2000) 97–113.
[15] I.G. Richardson, G.W. Groves, Models for the composition and structure of calcium silicate hydrate (C–S–H) gel in hardened tricalcium silicate pastes, Cem. Concr. Res. 22 (1992) 1001–1010.
[16] I.G. Richardson, G.W. Groves, Microstructure and microanalysis of hardened cement pastes involving ground granulated blast-furnace slag, J. Mater. Sci. 27 (1992) 6204–6212.
[17] I.G. Richardson, G.W. Groves, Microstructure and microanalysis of hardened ordinary Portland cement pastes, J. Mater. Sci. 28 (1993) 265–277.
[18] I.G. Richardson, G.W. Groves, The structure of the calcium silicate hydrate phases present in hardened pastes of white Portland cement/ blast-furnace slag blends, J. Mater. Sci. 32 (1997) 4793–4802.
[19] A. Plassais, M.-P. Pomiès, N. Lequeux, J.-P. Korb, D. Petit, F. Barberon, B. Bresson, Microstructure evolution of hydrated cement pastes, Phys. Rev., E 72 (2005) 041401.
[20] H. Van Damme.
[21] E.J. Verwey, Th.G. Overbeek, Theory of the Stability of Lyophobic Colloids, Elsevier, Amsterdam, 1948.
[22] B.V. Derjaguin, N.V. Churaev, V.M. Muller, Surface Forces, Consultants Bureau, New York, 1987.
[23] J. Israelachvili, Intermolecular and Surface Forces, 2nd ed. Academic Press, San Diego, 1992.
[24] D.F. Evans, H. Wennerström, The Colloidal Domain, 2nd ed. Wiley-VSH, NewYork, 1999.
[25] L. Guldbrand, B. Jönsson, H. Wennerström, P. Linse, Electrical double layer forces. A Monte Carlo study. J. Chem. Phys. 80 (1984) 2221–2228.
[26] R. Kjellander, S. Marcelja, Correlation and image charge effects in electric double layers, Chem. Phys. Lett. 112 (1984) 49–53 [Erratum, ibid. 114 (1985) 124].
[27] H. Van Damme, Et si Le Chatelier s'était trompé? Ann. Ponts Chaussées 71 (1994) 30–41.
[28] A. Meunier, Clays, Springer, Berlin, 2005.
[29] F. Bergaya, B.K.G. Theng, G. Lagaly (Eds.), Handbook of Clay Science, Elsevier, Amsterdam, 2006.
[30] R. Kjellander, S. Marcelja, R.M. Pashley, J.P. Quirk, Double-layer ion correlation forces restrict calcium-clay swelling, J. Phys. Chem. 92 (1988) 6489–6492.
[31] R. Kjellander, S. Marcelja, J.P. Quirk, Attractive double-layer interactions between calcium clay particles, J. Colliod Interface Sci. 126 (1988) 194–211.
[32] R.J.-M. Pellenq, A. Delville, H. van Damme, Cohesive and swelling behaviour of charged interfaces: a (N,V,T) Monte-Carlo study, in: B. McEnaney, T.J. Mays, J. Rouquerol, F. Rodriguez-Reinoso, K.S.W. Sing, K.K. Unger (Eds.), Characterization of Porous Solids IV, The Royal Society of Chemistry, Cambridge, 1997, pp. 596–603.
[33] R.J.-M. Pellenq, J.-M. Caillol, A. Delville, Electrostatic attraction between two charged surfaces: a (N,V,T) Monte Carlo simulation, J. Phys. Chem. 101 (1997) 8584–8594.
[34] R.J.-M. Pellenq, M. Crespin, N. Lequeux, C. Menager, L. Costalin, A. Delville, J.-M. Caillol, H. van Damme, A (NVT) Monte-Carlo study of the stability of charged interfaces. Application to cement and clay minerals, in: A. Nonat (Ed.), Hydration and Setting, RILEM Pub, Cachan, 2000, pp. 63–86.
[35] A. Delville, R.J.-M. Pellenq, Electrostatic attraction and/or repulsion between charged colloids, Mol. Simul. 24 (2000) 1–24.
[36] R.J.-M. Pellenq, H. van Damme, Why does concrete set? The nature of cohesion forces in hardened cement-based materials, MRS Bull. 29 (2004) 319–323.
[37] B. Jönsson, H. Wennerström, A. Nonat, B. Cabane, Onset of cohesion in cement paste, Langmuir 20 (2004) 6702–6709.
[38] B. Jönsson, A. Nonat, C. Labbez, B. Cabane, H. Wennerström, Controlling the cohesion of cement paste, Langmuir 21 (2005) 9211–921X.
[39] S. Lesko, E. Lesniewska, A. Nonat, J.C. Mutin, J.P. Goudonnet, Investigation by atomic force microscopy of forces at the origin of cement cohesion, Ultramicroscopy 86 (2001) 11–21.
[40] C. Plassard, E. Lesniewska, I. Pochard, A. Nonat, Nanoscale experimental investigation of particle interactions at the origin of the cohesion of cement, Langmuir 100 (2005) 7263–7270.
[41] P. Faucon, A. Delagrave, J.C. Petit, C. Richet, J.M. Marchand, H. Zanni, Interaction between salts (NaCl, CsCl) and calcium silicate hydrates (C–S–H), J. Phys. Chem., B 103 (1999) 7796–7802.
[42] A. Kalinitchev, R.J. Kirkpatrick, Molecular dynamics modeling of chloride binding to the surfaces of calcium hydroxide, hydrated calcium aluminate, and calcium silicate phases, Chem. Mater. 14 (2002) 3539–3549.
[43] H. Manzano, A. Ayuela, J.S. Dolado, On the formation of cementitious C–S–H nanoparticles, J. Comp.-Aided Mater. Design 14 (2007) 45–51.
[44] A. Gmira, Etude structurale et thermodynamique d'assemblages d'hydrates modèles du ciment. Thesis, University of Orléans, France (2003).
[45] A. Gmira, M. Zabat, R.J.-M. Pellenq, H. Van Damme, Microscopic physical basis of the poromechanical behavior of cement-based materials, Mater. Struct./Concr. Sci. Eng. 37 (2004) 3–14.
[46] R.J.-M. Pellenq, A. Gmira, H. van Damme, The Nature of Cohesion Forces in Hardened Cement-based Materials: The View from the Nanoscale, International Conference on Cement Chemistry, in: J.J. Beaudoin, J.M. Makar, L. Raki (Eds.), 12th International Congress on the Chemistry of Cement (CD), Cement Association of Canada, Montréal, 1997, pp. 596–603.
[47] S.A. Hamid, The crystal structure of the 11 Angström natural tobermorite, Z. Kristallogr. 154 (1981) 189–198.
[48] S. Merlino, E. Bonnaccorsi, T. Armbrumster, The real structure of tobermorite 11 Å: normal and anomalous forms, Eur. J. Mineral. 13 (2001) 577–590.
[49] E. Bonnaccorsi, S. Merlino, A.R. Kampf The crystal structure of tobermorite 14 Å (plombierite), a C–S–H phase, J. Am. Ceram. Soc. 88 (2005) 505–512.
[50] A.-L. Auzende, R.J.-M. Pellenq, B. Devouard, A. Baronnet, O. Grauby, Atomistic calculations of structural and elastic properties of serpentine minerals: the case of lizardite, Phys. Chem. Miner. 33 (2006) 266–275.
[51] B. Chen, J.R.G. Evans, Elastic moduli of clay platelets, Scripta Mater. 54 (2006) 1581–1585.
[52] R.J.-M. Pellenq, to be published.
[53] H. Sato, K. Ono, C.T. Johnston, A. Yamagishi, First-principles studies on the elastic constants of a 1:1 layered kaolinite mineral, Amer. Miner. 90 (2005) 1824–1826.
[54] P. Acker, Micromechanical analysis of creep and shrinkage mechanisms, in: F.-J. Ulm, Z.P. Bazant, F.H. Wittmann (Eds.), Creep, Shrinkage and Durability of Concrete and other Quasi-Brittle Materials, Elsevier, Oxford, UK, 2001.
[55] G. Constantinides, F.-J. Ulm, The effect of two types of C–S–H on the elasticity of cement-based materials: results from nanoindentation and micromechanical modelling, Cem. Concr. Res. 34 (2004) 67–80.
[56] G. Constantinides, F.-J. Ulm, The nanogranular nature of C–S–H, J. Mech. Phys. Solids 55 (2007) 64–90.
[57] I.N. Sneddon, The relation between load and penetration in the axisymmetric Boussinesq problem for a punch of arbitrary profile, Int. J. Eng. Sci. 3 (1965) 47–57.

[58] H.M. Jennings, A model for the microstructure of calcium silicate hydrate in cement paste, Cem. Concr. Res. 30 (2000) 101–116.
[59] H.M. Jennings, Colloid model of C–S–H and implications to the problem of creep and shrinkage, Mater. Struct./Concr. Sci. Eng. 37 (2004) 59–70.
[60] C. Plassard, E. Lesniewska, I. Pochard, A. Nonat, Intrinsic elastic properties of calcium silicate hydrates by nanoindentation, paper T2–03.4, in: J.J. Beaudoin, J.M. Makar, L. Raki (Eds.), Proceedings of the 12th International Congress on the Chemistry of Cement, Cement Association of Canada, Canada, 2007, (www.ICCC2007.org).
[61] This was first pointed out to us by George Scherrer.
[62] T.C. Powers, Structure and physical properties of hardened portland cement paste, J. Am. Ceram. Soc. 41 (1958) 1–6 and references therein.
[63] M. Zabat, M. Vayer, R. Harba, S. Bonnamy, H. Van Damme, Surface topography and mechanical properties of smectite films, Progr. Colliod and Polym. Sci. 105 (1997) 96–102.
[64] J. Minet, S. Abramson, B. Bresson, C. Sanchez, V. Montouillout, N. Lequeux, New layered calcium organosilicate hybrids with covalently linked organic functionalities, Chem. Mater. 16 (2004) 3955–3962.
[65] J. Minet, S. Abramson, B. Bresson, H. Van Damme, N. Lequeux, Organic calcium silicate hybrids: a new approach to cement-based nanocomposites, J. Mater. Chem. 16 (2006) 1379–1386.
[66] A. Franceschini, S. Abramson, B. Bresson, H. Van Damme, N. Lequeux, Cement-sylilated polymers nanocomposites. Paper W5-03.5, in: J.J. Beaudoin, J.M. Makar, L. Raki (Eds.), Proceedings of the 12th International Congress on the Chemistry of Cement, Cement Association of Canada, Canada, 2007, (www.ICCC2007.org).
[67] J. Kirkpatrick, K. Scrivener, Innovation in use and research on cementitious material, Cem. Concr. Res. 38 (2008) 128–136 (this issue).
[68] N.H. de Leeuw, J.W. Watson, S.C. Parker, Atomistic simulation of the effect of dissociative adsorption of water on the surface-structure and stability of calcium and magnesium oxide, J. Phys. Chem. 99 (1995) 17219–17225.
[69] M.T. Dove, T. Cool, D.C. Palmer, A. Putnis, E.K.H. Salje, B. Winkler, On the role of Al–Si ordering in the cubic-tetragonal phase transition of leucite, Am. Mineral. 78 (1993) 486–492.
[70] G.D. Price, S.C. Parker, in: E.K.H. Salje (Ed.), Physical Properties and Thermodynamic Behavio of Minerals, NATO ASI Series C, 225, 1988, pp. 591–618.
[71] B. Winkler, M.T. Dove, M. Leslie, Static lattice energy minimization and lattice-dynamics calculations on aluminosilicate minerals, Am. Mineral. 76 (1991) 313–331.
[72] D.R. Colins, C.R.A. Catlow, Computer simulation of structures and cohesive properties of micas, Am. Mineral. 77 (1992) 1172–1181.
[73] C.I. Saint-Diaz, A. Laguna-Hernandez, M.T. Dove, Modeling of dioctahedral 2:1 phyllosilicates by means of transferable empirical potentials, Phys. Chem. Min. 28 (2001) 130–141.
[74] N.H. de Leeuw, S.C. Parker, Molecular dynamics simulation of MgO surfaces in liquid water using a shell-model potential for water, Phys. Rev., B 58 (1998) 13901–13908.
[75] C. Pisani, Quantum mechanical *ab initio* calculation of the properties of crystalline materials, Lecture in Chemistry, 177, Springer, 1996.
[76] P. D'arco, M. Causa, C. Roetti, B. Silvi, Periodic Hartree–Fock study of a weakly bonded layer structure-brucite, Phys. Rev., B 47 (1993) 3522–3529.